Stefan Gerlach*, Maximilian Neidhardt*, Thorben Weiß, Max-Heinrich Laves, Carolin Stapper, Martin Gromniak, Inga Kniep, Dustin Möbius, Axel Heinemann, Benjamin Ondruschka, and Alexander Schlaefer

Needle insertion planning for obstacle avoidance in robotic biopsy

https://doi.org/10.1515/cdbme-2021-2199

Abstract: Understanding the underlying pathology in different tissues and organs is crucial when fighting pandemics like COVID-19. During conventional autopsy, large tissue sample sets of multiple organs can be collected from cadavers. However, direct contact with an infectious corpse is associated with the risk of disease transmission and relatives of the deceased might object to a conventional autopsy. To overcome these drawbacks, we consider minimally invasive autopsies with robotic needle placement as a practical alternative. One challenge in needle based biopsies is avoidance of dense obstacles, including bones or embedded medical devices such as pacemakers. We demonstrate an approach for automated planning and visualising suitable needle insertion points based on computed tomography (CT) scans.

Needle paths are modeled by a line between insertion and target point and needle insertion path occlusion from obstacles is determined by using central projections from the biopsy target to the surface of the skin. We project the maximum and minimum CT attenuation, insertion depth, and standard deviation of CT attenuation along the needle path and create two-dimensional intensity-maps projected on the skin. A cost function considering these metrics is introduced and minimized to find an optimal biopsy needle path. Furthermore, we disregard insertion points without sufficient room for needle placement. For visualisation, we display the color-coded cost function so that suitable points for needle insertion become visible.

We evaluate our system on 10 post mortem CTs with six biopsy targets in abdomen and thorax annotated by medical experts. For all patients and targets an optimal insertion path is found. The mean distance to the target ranges from (49.9 ± 12.9) mm for the spleen to (90.1 ± 25.8) mm for the pancreas.

Keywords: robotics, biopsy, forensic medicine, needle placement, path planning

***Equal contribution**

Stefan Gerlach, Maximilian Neidhardt, Max-Heinrich Laves, Carolin Stapper, Martin Gromniak, Alexander Schlaefer, Institute of Medical Technology and Intelligent Systems, Hamburg University of Technology, Hamburg, Germany, e-mail: stefan.gerlach@tuhh.de

Thorben Weiß, Inga Kniep, Dustin Möbius, Axel Heinemann, Benjamin Ondruschka, Institute of Legal Medicine, University Medical Center Hamburg-Eppendorf

1 Introduction

Studying pathological tissue changes during a pandemic, such as COVID-19 can be valuable for treatment and diagnostic of infections [5]. Commonly, samples from any body tissue can be preserved from a corpse during a conventional autopsy. However, drawbacks are the risk of disease transmission, non-consent by relatives and limited human resources during a pandemic. We consider minimally invasive needle biopsy with a robotic arm as an alternative approach. Robots allow accurate needle positioning and the corpse can be encased by a protective body bag during the whole procedure, reducing the risk of disease transmission. First, the physician chooses a biopsy target based on a post mortem computed tomography (CT) scan. Next, a suitable insertion path needs to be defined. Conventionally a desired insertion path is located in an oblique slice of the CT, making it challenging and time consuming for the physician to verify a collision-free needle path to the target.

Several methods for planning assistance in radiofrequency ablation have been published [1, 7] including visualising needle paths without obstructions inside 2-dimensional CT slices [8]. Furthermore, path planning for a robot inside a virtual simulation environment has been studied [2]. Still, tissue extraction from corpses includes novel access points to biopsy targets which might not be feasible in a clinical biopsy. In our previous research we have placed medical biopsy needles with robots and sensed the forces acting in human corpse tissue [3].

In this study we extend our approach by finding optimal needle insertion paths and demonstrate an intuitive way for needle path planning for realising tissue extraction with a robot during a pandemic. We present a method to project information of the needle path onto a three-dimensional rendering of the skin of the corpse. We study different metrics representing the different objectives when choosing a suitable needle path. Each metric can be displayed individually when desired by the physician. Our method is evaluated on CT scans of COVID-19 and non-COVID-19 corpses where desired tissue targets for minimally invasive biopsies are annotated by medical experts of the Institute of Legal Medicine. We estimate the cost for all possible needle insertion points on the surface for an individual target and propose a suitable needle insertion point to the physician.

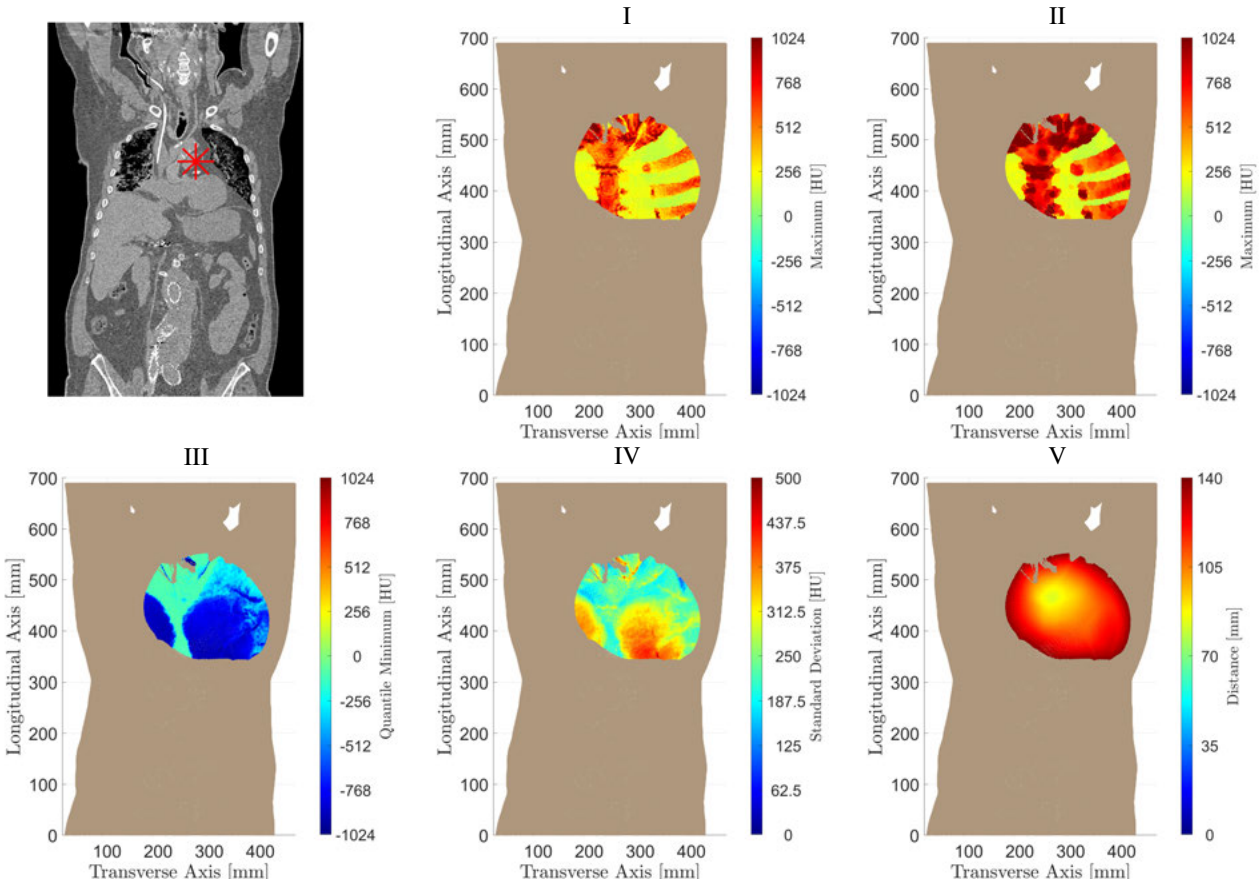

Fig. 1: Projections of needle insertion positions on the skin. **Top Left:** Annotated target by physician (aorta pulmonalis). **Projections:** All feasible insertion positions on the skin are given for a 140 mm biopsy needle. The projections are estimated for each needle insertion path as the (I) maximum Hounsfield unit (HU), (II) maximum HU with increased bone size, (III) minimum HU quantile, (IV) standard deviation and (V) the distance between target and surface point.

2 Methods

2.1 Data and annotation

Our approach has been evaluated on CT scans of ten corpses covering a wide range of body types (Tab. 1). Biopsy targets are annotated by medical experts in CT slices for extracting tissue of the right lobe of the liver (transabdominal), kidney (left intercostal), spleen (intercostal), pancreas (transabdominal), hilar lymph nodes (substernal) and pulmonary aorta (intercostal).

2.2 Identification and visualization of needle insertion paths

We visualize suitable linear access paths to the physician in a three-dimensional rendering. We present several colormaps which represent metrics based on the intensity values along a needle trajectory.

Skin Segmentation

We employ Python and Numpy [4] to implement the projection of CT intensities along straight lines from the annotated biopsy target to the surface of the skin. First, we detect the largest connected tissue volume by using a threshold based segmentation of the CT voxel values. We then apply a closing function with a kernel size of 1 cm to this volume to close natural openings such as mouth and nose. The resulting volume might still contain air inclusion such as in the lung or the bowel. Hence, we further refine our volume by segmenting the air surrounding the body. Therefore, we invert our tissue volume segmentation and define the largest remaining continuous volume as the surrounding air. Now we invert the air volume to produce a solid segmentation of the body. Finally, we select the surface of the solid segmentation as the surface of the body. Note, we do not explicit segment the tissue to air boundaries since it is computational inefficient.

Tab. 1: Post mortem CT datasets evaluated in this study. COVID-19 refers to a laboratory- confirmed SARS CoV-2-infection detected.

Patient	P1	P2	P3	P4	P5	P6	P7	P8	P9	P10
Gender, Age	f, 88	f, 63	m, 74	m, 74	m, 78	m, 78	m, 58	f, 95	m, 81	m, 78
Height	158 cm	177 cm	179 cm	183 cm	180 cm	170 cm	177 cm	150 cm	180 cm	182 cm
Weight	59.2 kg	96.0 kg	104.0 kg	87.7 kg	113.3 kg	73.5 kg	62.7 kg	32.1 kg	81.4 kg	100.0 kg
BMI	23.7	30.6	32.5	26.2	35.0	25.4	20.0	14.3	25.1	30.2
COVID-19	neg.	neg.	neg.	neg.	neg.	neg.	neg.	pos.	pos.	pos.

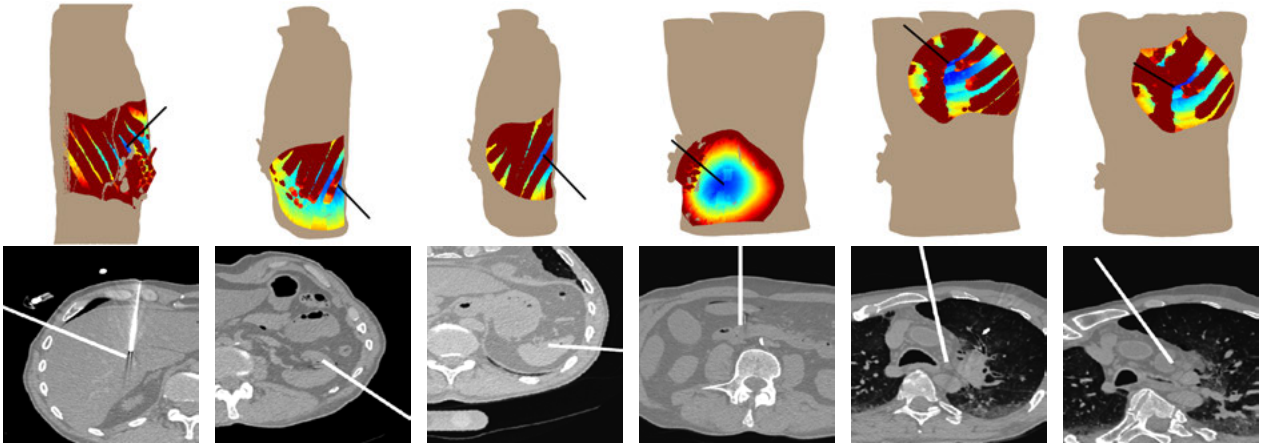

Fig. 2: Cost maps for needle insertions demonstrated on corpse P7. Given is the cost map in the top row with red indicating a "high" cost and blue indicating a "low" cost for an entry point. The proposed needle insertion path is given in the bottom row to the corresponding target in the top row. Please note that the CT slices are oblique to image the proposed needle trajectory. The targets are from left to right column: liver right lobe, left kidney, spleen, pancreas, hilar lymph nodes and pulmonary aorta.

Needle Insertion Points

We reduce the number of feasible insertion points on the skin depending on the target location. First, we only estimate our metrics on surface points, which can be reached by the given needle length. Second, we disregard surface points if more tissue is beyond the surface point on the same line connecting the target and the surface point. This could be the case for example if an arm is positioned next to the corpse or because of a skin fold and needle placement would not be possible. By removing these points we can further increase our computation time.

Overlay Metrics

We estimate metrics along the line connecting the biopsy target and the refined skin projections. The metrics are the following:

- The *maximum* CT intensity (CT_{max}) allows conclusions about the location of dense structures such as bones. Naturally, these should be avoided during insertions.
- We further refine CT_{max} by increasing the size of dense structures to avoid bone punctures.
- Avoiding crossing pleural space in case of non- pulmonary tissues is recommended [6]. Hence, we estimate the amount of air cavities along the needle path. We define this metric as the projection of the maximum of the *5 % quantile* of CT intensities CT_{qmin} along the needle path.
- Since more homogeneous tissue can allow for more accurate path planning we also project the *standard deviation* of CT intensities (CT_{sd}).
- The *distance* to the target from the insertion points (CT_{d}). A shorter needle insertion distance leads to less trauma and is therefore preferable [6].

We linearly combine these metrics with

$$OV = \alpha \cdot CT_{\text{max}} + \beta \cdot CT_{\text{qmin}} + \gamma \cdot CT_{\text{sd}} + \delta \cdot \hat{d}\,, \qquad (1)$$

where the weighting factors $\alpha + \beta + \gamma + \delta = 1$. We normalize d to the range of CT_{max} for $\hat{d}$ to allow for more intuitive interpretation of the weighting factors. Fig. 1 shows the resulting metrics as overlays onto the surface of the segmentation.

3 Results

We evaluate the optimization of the insertion path for 10 post mortem CTs. We set $\beta = 0$, $\gamma = 0$, $\alpha = 0.8$, and $\delta = 0.2$ and consider a standard length for a clinical biopsy needle "140 mm" long needle. For every patient, overlays are generated automat-

Tab. 2: Overview of metrics for optimal insertion points for all evaluated biopsy targets and patients (Tab. 1) representing small, medium, and large BMI. Given is the minimal cost for the distance to the target (*OV*), the minimal cost for the maximum projected HU value (*CT max* [HU]) and the distance to the target for the point with the minimal cost for patients (d [mm]), average and standard deviation, and correlation with the patient's BMI. The evaluated target tissues are: (A) liver, (B) kidney, (C) spleen, (D) pancreas, (E) hilar lymph nodes, and (F) pulmonary aorta

Target	Metric	P3	P6	P8	Average	Cor
	OV	161.8	107.2	75.6	125.4 ± 31.4	0.71
A	CT_{max}	197.0	134.0	92.0	141.1 ± 30.9	0.72
	d	80.8	92.0	61.8	82.5 ± 20.3	0.34
	OV	128.2	96.0	88.2	121.4 ± 50.0	0.58
B	CT_{max}	155.0	107.0	99.0	132.7 ± 58.4	0.61
	d	73.4	60.0	48.9	76.7 ± 23.3	0.83
	OV	134.6	99.2	88.7	112.0 ± 31.6	0.66
C	CT_{max}	165.0	124.0	89.0	125.9 ± 39.7	0.73
	d	44.7	51.0	24.5	49.9 ± 13.0	0.65
	OV	166.1	39.6	46.7	90.1 ± 39.2	0.70
D	CT_{max}	207.0	33.0	57.0	101.7 ± 49.7	0.54
	d	98.4	75.2	65.3	90.1 ± 25.8	0.74
	OV	125.9	86.7	61.7	134.2 ± 76.1	0.70
E	CT_{max}	122.0	99.0	76.0	133.8 ± 65.3	0.72
	d	99.8	88.1	61.0	89.6 ± 11.8	0.79
	OV	167.3	108.2	76.0	127.6 ± 91.8	0.41
F	CT_{max}	154.0	133.0	86.0	108.4 ± 56.5	0.36
	d	86.4	82.0	43.1	83.3 ± 16.6	0.66

ically without adjusting parameters with a total computation time of less than 60 s on CT resolution.

Fig. 2 shows an example of resulting cost maps and optimal insertion paths for one patient and every target studied. The oblique slices show that obstacles are avoided and a short path is selected to reach the target. The resulting metrics for the optimal insertion paths according to the combined optimization function are shown in Tab. 2. We estimate the pearson correlation Cor to find the relationship between body type and evaluated metrics.

4 Discussion

We presented a system for automatically visualising and optimising needle insertion paths. Considering the resulting metrics of the optimal insertion point, while differences between biopsy targets and patients in the $CT_{\max}$ can be observed, all targets can be reached while avoiding bony structures. However, especially for targets in the pancreas, hilar lymph nodes, and pulmonary aorta, the standard deviation is high relative to the mean, indicating a large variability in tissue properties which needs to be taken into account when advancing the needle to the target.

5 Conclusion

In this work, a method for visualising and optimising needle insertion paths for robotic needle insertion is presented. A preliminary retrospective study shows that optimal needle paths can have a large variability depending on the target and the physique of the patient. This system represents a step towards automatic robotic needle interventions in the post-mortem setting and allows for autonomous insertion path selection.

Author Statement

Research funding: This research is partially funded by the DEFEAT PANDEMIcs project from the Bundesministerium für Bildung und Forschung (BMBF) under grant agreement no 01KX2021 and partially by the DFG SCHL 1844/2-2 project. Conflict of interest: Authors state no conflict of interest. Informed consent: Informed consent has been obtained for all cases included in this study. Ethical approval: The Ethics Committee of the Hamburg Chamber of Physicians approved the study (No.: 2020-10353-BO-ff).

References

[1] S. M. Bakhshmand, R. Eagleson, and S. de Ribaupierre. Multimodal connectivity based eloquence score computation and visualisation for computer-aided neurosurgical path planning. *Healthc Technol Lett*, 4(5):152–156, 2017.

[2] E. Belbachir, E. Golkar, B. Bayle, and C. Essert. Automatic planning of needle placement for robot-assisted percutaneous procedures. *Int J Comput Assist Radiol Surg*, 13(9):1429–1438, 2018.

[3] M. Gromniak, M. Neidhardt, A. Heinemann, K. Püschel, and A. Schlaefer. Needle placement accuracy in CT-guided robotic post mortem biopsy. *Curr Dir Biomed Eng*, 6(1):20200031, 2020.

[4] C. R. Harris, K. J. Millman, and S. J. van der Walt et al. Array programming with NumPy. *Nature*, 585(7825):357–362, 2020.

[5] I. Kniep, A. Heinemann, C. Edler, J. Sperhake, K. Püschel, B. Ondruschka, and A. Schröder. Covid-19 lungs in post-mortem computed tomography. *Rechtsmedizin*, 31(2):145–147, 2021.

[6] J. Lorenz and M. Blum. Complications of percutaneous chest biopsy. *Semin Intervent Radiol*, 23(2):188–193, 2006.

[7] R. Khlebnikov, B. Kainz, J. Muehl, and D. Schmalstieg. Crepuscular rays for tumor accessibility planning. *IEEE Trans Vis Comput Graph*, 17(12):2163–2172, 2011.

[8] C. Schumann, J. Bieberstein, S. Braunewell, M. Niethammer, and H.-O. Peitgen. Visualization support for the planning of hepatic needle placement. *Int J Comput Assist Radiol Surg*, 7(2):191–197, 2012.